THE UPGRADED OUTER EM CALORIMETER OF FOCUS AT FERMILAB

S. Bianco F.L. Fabbri M. Giardoni
L. Passamonti V. Russo S. Sarwar A. Zallo
Laboratori Nazionali di Frascati - via E. Fermi 40, I-00044 Frascati, Italy
S. Carrillo H. Mendez
CINVESTAV-IPN, Dept. of Physics, 07000 México, DF
G. Gianini
Dip. di Fisica Nucleare e Teorica dell'Univ. and INFN, I-27100 Pavia, Italy
J. Anjos I. Bediaga C. Gobel A. Laudo J. Magnin
J. Miranda I. Pepe F. Simão A. Sanchez A. Reis
CBPF - R. Dr. X.Sigaud 150, BR-22290-180 Rio de Janeiro, RJ

Abstract

Operational performance, algorithms, stability and physics results of the Outer em calorimeter of FOCUS are overviewed.

1 Introduction and historical overview

FOCUS is a heavy-flavor photoproduction experiment located at the Wide Band Photon Area of Fermilab. An upgraded version of its predecessor E687[1], FOCUS is composed of (Fig.1) a μstrip silicon detector, a large acceptance magnetic spectrometer with MWPC, Cherenkov differential counters, muon detectors, hadron calorimetry, and both forward (Inner em), and large angle (Outer em) electromagnetic calorimetry. The topics in charm physics that are being investigated include lifetimes, semileptonic decays, charm baryons, charm spectroscopy, searches for $D^0 - \bar{D}^0$ mixing and for rare and forbidden decays, charmonium production and radiative decays, and charm meson and baryon decays with neutrals.

The experiment was designed starting in 1981; in 1985 there was the first test beam of the completed spectrometer; in 1987 the first E687 data-taking period, interrupted by a fire. The spectrometer was seriously damaged, but quickly repaired. In 1990-1991 the second E687 data taking took place. In 1995 the E687 spectrometer became FOCUS and underwent upgrades, with the Outer em calorimeter being equipped with a new plane of square scintillator tiles. The 1996-1997 FOCUS data-taking period met the goal of collecting ten times the E687 statistics of reconstructed charm decays, by fully reconstructing more than ten million charm particle decays.

2 Physics requirements, geometry acceptances

The Outer em calorimeter (Fig. 2a) is located $900\,\mathrm{cm}$ from the target. Its external dimensions are $(255 \times 205)\,\mathrm{cm}^2$, with an internal rectangular aperture $(51 \times 88)\,\mathrm{cm}^2$. This corresponds to an angular acceptance for photons $(28 \leq |\theta_x| \leq 142)\,\mathrm{mrad}$, $(49 \leq |\theta_y| \leq 114)\,\mathrm{mrad}$. A vertical gap, set at $9\,\mathrm{cm}$ for the 1996-97 run, avoids showers from the most abundant background process, i.e., Bethe-Heitler e^+e^- pair production. The Outer em is required to reconstruct γ-initiated showers from charm radiative and π^0 decays in the energy range $(0.5 \leq E_\gamma \leq 15)\,\mathrm{GeV}$ and to perform e/π identification for charm semi-electronic decays in the momentum range $(2.5 \leq P \leq 20)\,\mathrm{GeV/c}$, thus extending the Cherenkov counter identification, which is limited to $P < 6\,\mathrm{GeV/c}$. Some μ/π identification power is expected to help identify low-momentum muons in charm semimuonic decays. Typical geometrical acceptances range from 30% for electrons and muons in charm meson semileptonic decays, and 40-50% for decays with one or more π^0 in the final state, including the case of shared π^0 (one γ in the Inner and one in the Outer em calorimeter).
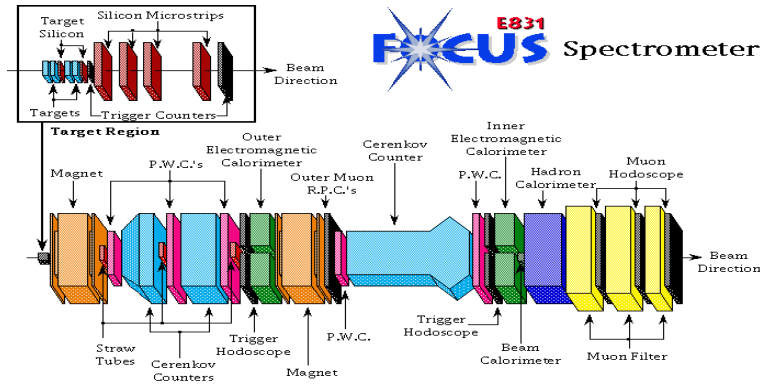
Figure 1: The FOCUS (E831) spectrometer at the Fermilab Wide Band Photon Beam.

3 Mechanical structure

The Outer em calorimeter is made of Pb plates (stiffened with a 6% Sb by weight) and scintillator layers (POPOP, $C_{24}H_{12}N_2O_2$ doped with 8% naphtalene, and NE-102 were used), for a total of $19\,X_0$ and $1.4\,\lambda_i$ (Tab.1). Scintillator layers are made of strips, whose light readout is either individual (OE0, OE9 segments) or five-fold integrated by a light guide to a single PM (all other segments), for a total of 1136 readout channels. Each counter in the calorimeter is individually wrapped in $0.1\,mm$ Al foils and black plastic. Horizontal and vertical five-fold counters are interlaced as shown in Fig.2 b). The counters are arranged in nine independent views along Z (Z is the beam direction), and four independent quadrants in the (X,Y) plane. A module of S-Z strips $(45^o - 135^o)$ performs horizontal-vertical matching of clusters. The counters are equipped with ten-stage, EMI-9902KB photomultiplier tubes (PMT) operating at a typical gain of 10^6 at $1000\,V$, with a quantum efficiency of 20% at $440\,nm$, which were individually tested in order to select only those with good linearity and small sensitivity to rate effect[2]. The PMT's are powered by LeCroy 1440 and custom-made FRAMM[3] HV systems, via a high-linearity, anode grounded voltage divider supplying $1.5\,mA$ at $1500\,V$. The PMT signals reach the counting room via $60\,m$ long coaxial cables, where they are converted by a Lecroy 1881M Fastbus ADC, with a $0.050\,pC/count$ conversion. The Outer em calorimeter can be displaced both horizontally and vertically for calibration and access purposes.

A scintillator tile array module recovers showers in the small-angle, high-occupancy region, improves horizontal-vertical matching, and cleans the π^0 peak by rejecting fake matches. The module is located at shower max, i.e., between the OE1 and OE2 modules, and is composed of an array of 100 supertiles, and edge counters to flag laterally noncon-

E831 FOCUS Outer em calorimeter
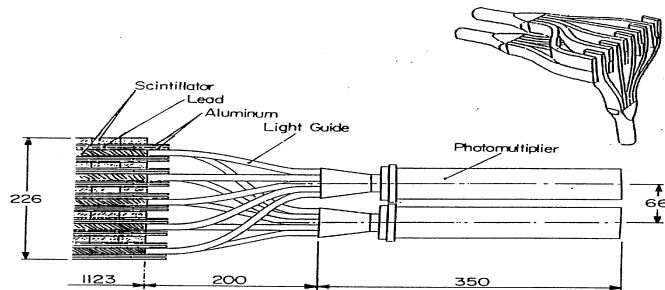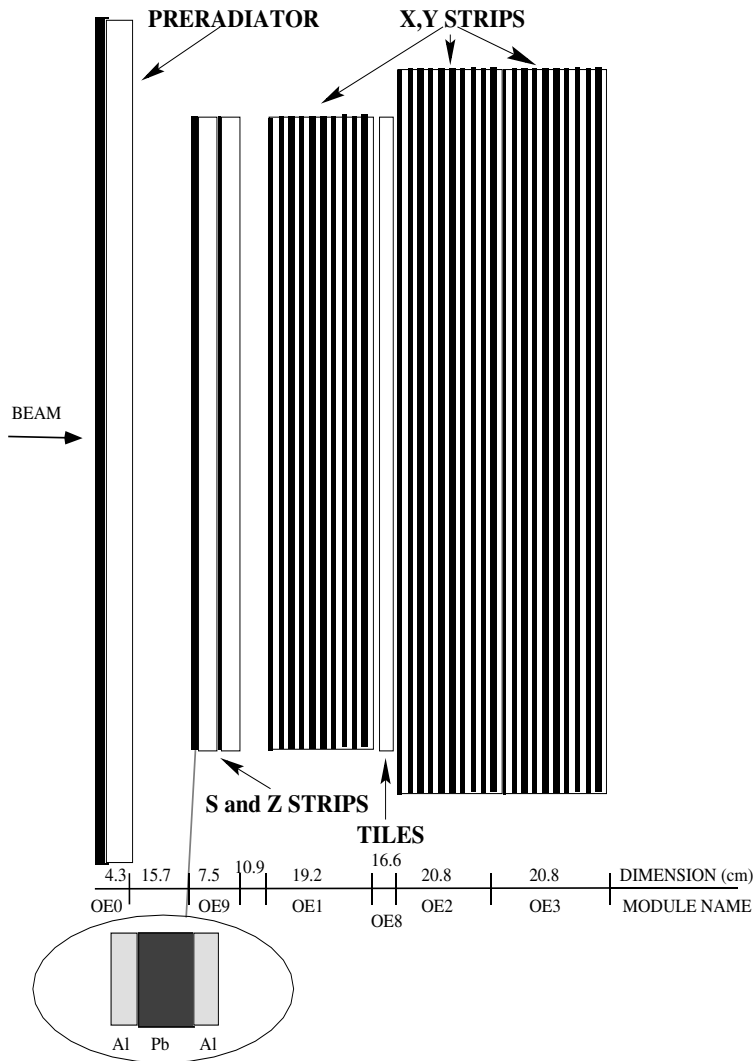
ELEVATION VIEW (NOT TO SCALE)

PRERADIATOR   **X,Y STRIPS**

BEAM

S and Z STRIPS

TILES

4.3	15.7	7.5	10.9	19.2	16.6	20.8	20.8	DIMENSION (cm)
OE0		OE9		OE1	OE8	OE2	OE3	MODULE NAME

Al Pb Al

Scintillator
Lead
Aluminum
Light Guide

Photomultiplier

226

1123   200   350

66

Figure 2: a) The Outer em calorimeter longitudinal structure showing the sandwich of absorber and scintillator planes. b) X and Y strip planes interlaced and five-fold integrated to a readout PMT (dimensions are millimeters).

4

Table 1: Longitudinal segmentation and counter geometry of the Outer em calorimeter.

|	OE0	OE9S	OE9Z	OE1V	OE1H
X_o sampled	0-1.3	1.3-1.9	1.9-2.5	2.5-7.3	3.0-7.8
λ_i sampled	0-.09	.09-.15	.15-.21	.21-.56	.25-.60
Sandwich struct.	AlPbAlSc			5×(AlPbAlSc)	
Pb thick. [cm]	0.650	0.254			
Al thick. [cm]	0.254				
Scint. type	NE102	POPOP			
Scint. thick. $[cm]$	3.0			1.0	
Counter width $[cm]$	3.3	7.0		3.3	
Counter hor.	hor	45°	135°	vert	hor
Counters integrated	1			5	
	OE8T	OE2V	OE2H	OE3V	OE3H
X_o sampled	7.8-7.9	7.9-12.7	8.4-13.3	13.3-18.2	13.7-18.6
λ_i sampled	.60-.61	.61-.96	.65-1.1	1.1-1.4	1.14-1.44
Sandwich struct.	AlScScAl	5×(AlPbAlSc)			
Pb thick. [cm]	-	0.254			
Al thick. [cm]	0.254				
Scint. type	BC404-B	POPOP			
Scint. thick. $[cm]$	0.5	1.0			
Counter width $[cm]$	10.0	3.3			
Counter hor.	sqr	vert	hor	vert	hor
Counters integrated	2	5			
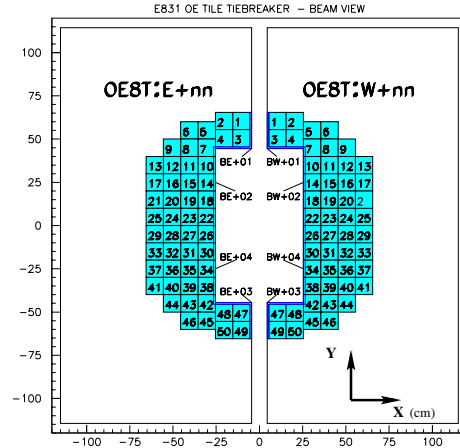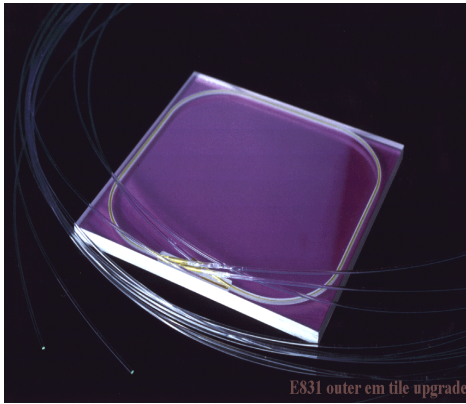
Figure 4: left) A complete tile counter before wrapping; right) layout of tile counter array, and edge counters.

tained showers. Each supertile is made of two $(10 \times 10 \times 0.5)\,\mathrm{cm}^3$ tiles (BICRON BC404-B scintillator), each is equipped with two 20 cm-long, 1-mm-diameter wavelength shifting (WLS) optical fibers (Kuraray Y11 multiclad S-type) 20 cm-long, α-cut, with all four ends thermally spliced to 2 m-long clear fibers following the CDF endplug splicing technique [4], with a heat-shrinking tube to protect the splice. The eight ends of the clear fibers of each supertile are optically coupled by means of optical grease to a EMI-9902KB PMT.

Each tile is wrapped in white Teflon tape, and the side is painted with white reflective paint by BICRON. The tile array is enclosed in a light-tight Al case. The light transmission efficiency of the thermal splice was measured on relevant samples during the splicing process and shown to be typically 94%.

Figure 3: Light attenuation curves for three different sized strip counters.

4 Equalization with mips

Beam halo muons were used to determine the counter geometry, for an approximate PMT gain balancing ($\pm 10\%$), to determine the light attenuation curves inside strips (Fig.3), and the equalization constants. The light output was measured in the laboratory with cosmic rays to be 30 photoelectrons/mip for a supertile, and 100 photoelectrons/mip for a five-fold counter at $20\,\mathrm{cm}$ from PMT. The relative width fwhm of the energy distribution for a mip
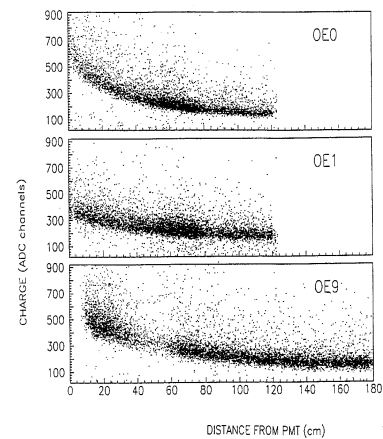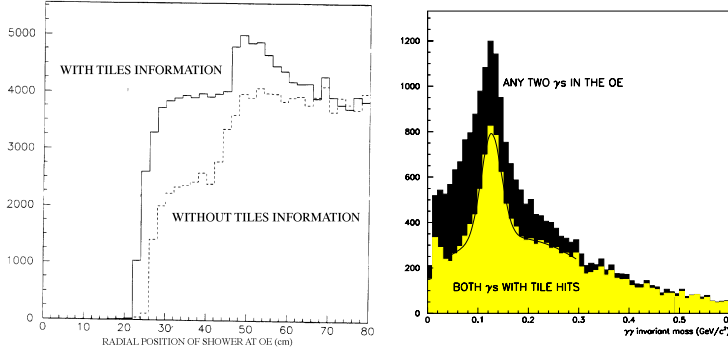
6

Figure 5: (a) Loss of reconstruction efficiency in the small-angle region of the Outer em calorimeter; (b) $\gamma\gamma$ invariant mass peak with and without tile array hit confirmation.

is 40% for a supertile, and 30% for a five-fold counter.

5   Shower reconstruction strategy

The reconstruction algorithm begins with the identification of clustered energy deposits. Clusters of energy deposits associated with the projection of charged tracks reconstructed in the magnetic spectrometer are tagged. The reconstruction of neutral showers uses the remaining clusters. Energy deposits (in ADC counts units) for each counter are multiplied by the mip equalization constants, and then summed up to determine the detected energy associated to each cluster.

Pairs of clusters in the two orthogonal X-Y views of each OE segment are formed using the energy balance as a criterium, after proper weighing for light attenuation inside the strip counters. Neutral showers are formed by aligned X-Y pairs in the different OE segments. The diagonal counters and the tiles are used to resolve ambiguities. The use of tile array information improves the efficiency of X-Y matching in the small angle region (Fig.5a) by reducing the number of fake matches (Fig.5b).

The coordinates of the shower centroids are determined considering the energy deposited in each counter of the X-Y pairs. Once corrected for systematic effects (§ 6), the shower centroids determine the photon incidence point. The π^0 invariant mass is computed by the measurement of relative angle and energy of the decay photons. When computing the invariant mass of higher states with one or more π^0 in the final state, the π^0 invariant mass is fixed at its nominal rest value, and the photon momenta are rearranged by means of a 1-C fit. The classical algorithm in Ref.[7] was modified in order to take

7

into account space resolution[8].

Neutral showers are identified as em or hadronic by means of the Discriminant Analysis algorithm (§ 7). Finally, the sum of energy clusters longitudinally forming a reconstructed photon track gives the detected energy $E_{detected}$. The reconstruction efficiency for single isolated showers was measured using primary Bethe-Heitler e^+e^- pairs. The e^+e^- tracks found in the proportional chambers were projected onto the OE front. Shower reconstruction was then performed using all the available clusters. The efficiency for reconstructing the shower associated with the electron or positron track was greater than 95% over the range $2 - 20\,\mathrm{GeV}$, and better than 90% over the range $0.5 - 2\,\mathrm{GeV}$.

6 Energy calibration, linearity, energy and space resolution

The response of the calorimeter to photon- and electron-initiated e.m. showers, the scale factor α between detected energy and incident energy, and the energy resolution have been studied using a GEANT simulation. Simulation predictions have been verified with e^+e^- pairs and electron beam in calibration runs, e^+e^- pairs from the process $\pi^0 \rightarrow \gamma\gamma, \gamma\mathcal{N} \rightarrow e^+e^-$ of photon conversion in physics events for electron-initiated showers constants , and π^0 peaks for photon-initiated showers constants and absolute calibration of the energy scale.

The detected energy is parametrized as $E_{detected} = E/\alpha$ where E is the particle incident energy and $E_{detected}$ is the particle energy deposited in the calorimeter active layers. Energy linearity and resolution are shown in Fig.6, in agreement with the simulation predictions.

The photon impact point X_{true} is determined from the em shower center-of-gravity $X_{cog} \equiv 2\Delta \sum iX_iA_i / \sum iA_i$, where $2\Delta = 3.3\,\mathrm{cm}$ is the counter width, after applying the standard correction[5] $X_{true} = b \arcsinh\left(\frac{X_{cog}}{\Delta}\sinh\frac{\Delta}{b}\right)$ After correction, we determine the space resolution as from e^+e^- calibration events (Fig.7) to be $\sigma(X_{true}) = \pm 0.3\,\mathrm{cm}$ in the energy range $(1 \leq E_\gamma \leq 20)\,\mathrm{GeV}$.

7 Particle ID

The Outer em calorimeter extends the e/π rejection beyond the Cherenkov momentum range, i.e., from 6 to 20 GeV/c. The identification algorithms have been developed in the framework of the Discriminant Analysis[6], which allows one to distinguish between two or more groups of events. As first step, we determine a set of N variables $V_{1,N}$ *(Discriminant Variables)*, significantly different among the M groups of events $(\{A_j\}, \quad j = 1, M)$ to be distinguished (Fig.8). A typical set of variables is composed of the ratio E/P be-
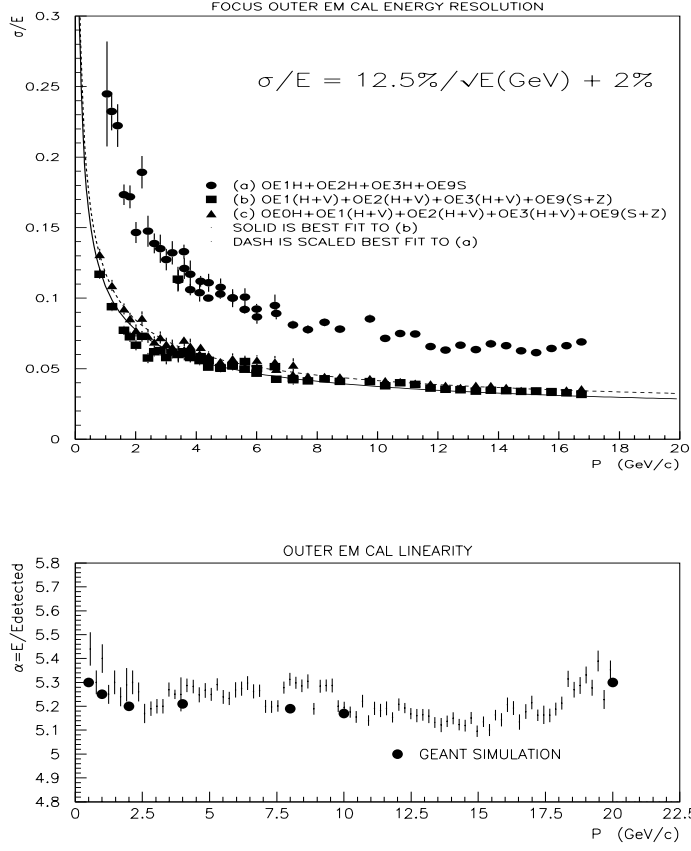
Figure 6: Energy resolution (with the constant term added in quadrature) and linearity as measured by calibration e^+e^- pairs.

tween the energy measured by the calorimeter and the track momentum by the tracking system, the lateral and longitudinal shower development pattern, the cluster centroid residuals and widths. Next, the *score* function $S_A = \sum_{i=1,N} c_i V_i$ is built, and we find coefficients c_i which maximize separation among the S_A, thus applying one cut on S (Fig.9a). As training samples of known membership we used e^+e^- Bethe-Heitler pairs embedded in hadronic events, pions from $K_S \rightarrow \pi^+\pi^-$ decays, and muons from dedicated runs with beamdump. The overall pion residual contamination obtained for an 85% electron efficiency is 10^{-2}, while the pion residual contamination is 10^{-1} for 85% muon efficiency (Fig.9b). Efficiency for muons from J/ψ decay, and rejection of pions compared with the Outer muon detector performances are shown in Fig.11 a,b).
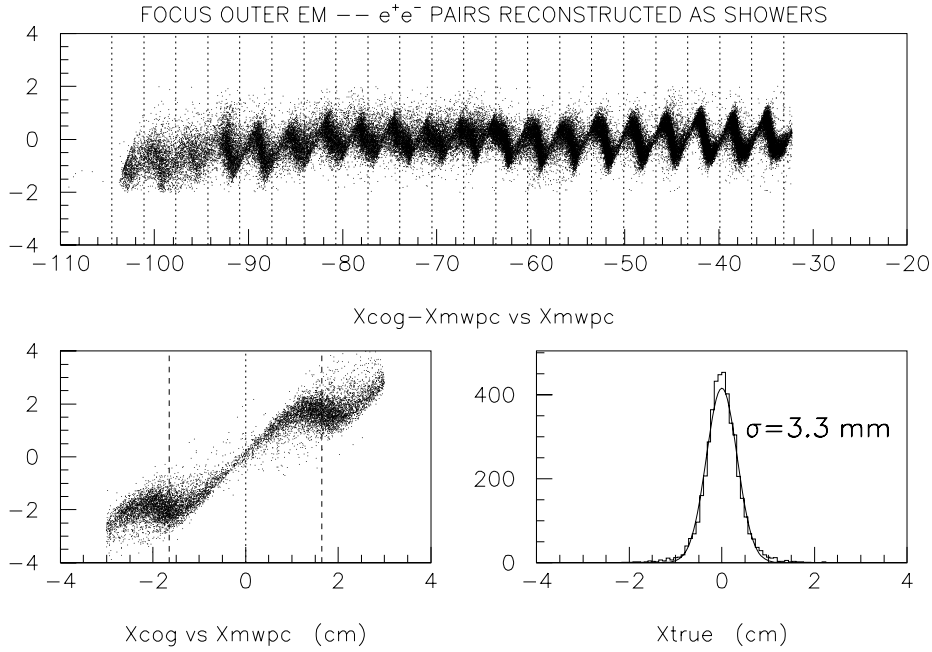
9

Figure 7: a,b) Shower center-of-gravity X_{cog} as measured for a beam of calibration electrons sweeping the Outer em at increasing angles. The calorimeter response degrades when the em shower reaches the lateral boundary of the detector acceptance, thus losing full lateral containment. c) Distribution of residuals after correction.

8 Long-term stability

The calorimeter stability is controlled by monitoring the ADC pedestals between spills, the PMT HV supplies, and the single-channel rough response by a N_2 laser light source[9]. The availability of a muon beam halo over the entire area of the Outer em allows muon calibrations to be performed regularly. The long-term, fine-grained run-dependent stability is given by exploiting physical signals in events, namely

1. $\pi^0 \rightarrow \gamma\gamma$ (Fig.10 a)

2. E/P for electrons (e^+e^- Bethe-Heitler pairs embedded in hadronic events, Fig.10 b)

3. $\pi^0 \rightarrow \gamma\gamma$, with one γ conversion $\gamma\mathcal{N} \rightarrow e^+e^-$ (Fig.10 c)

Results are summarized in Fig.10 d,e,f. Electron and π^0 signals in hadronic events (Fig.10 b,a) can track the shifts in detector response up to a stability of $\pm1\%$ over the entire
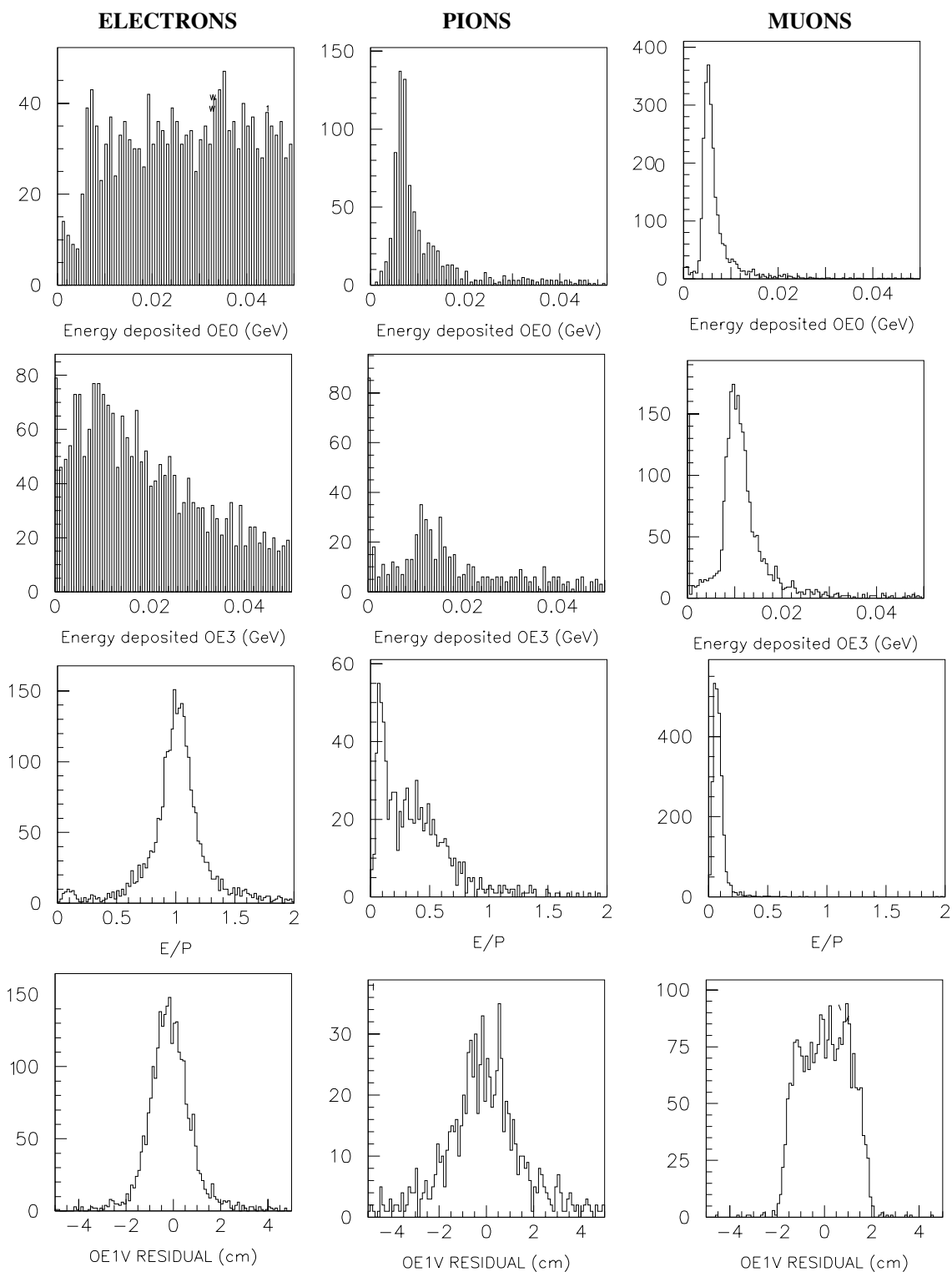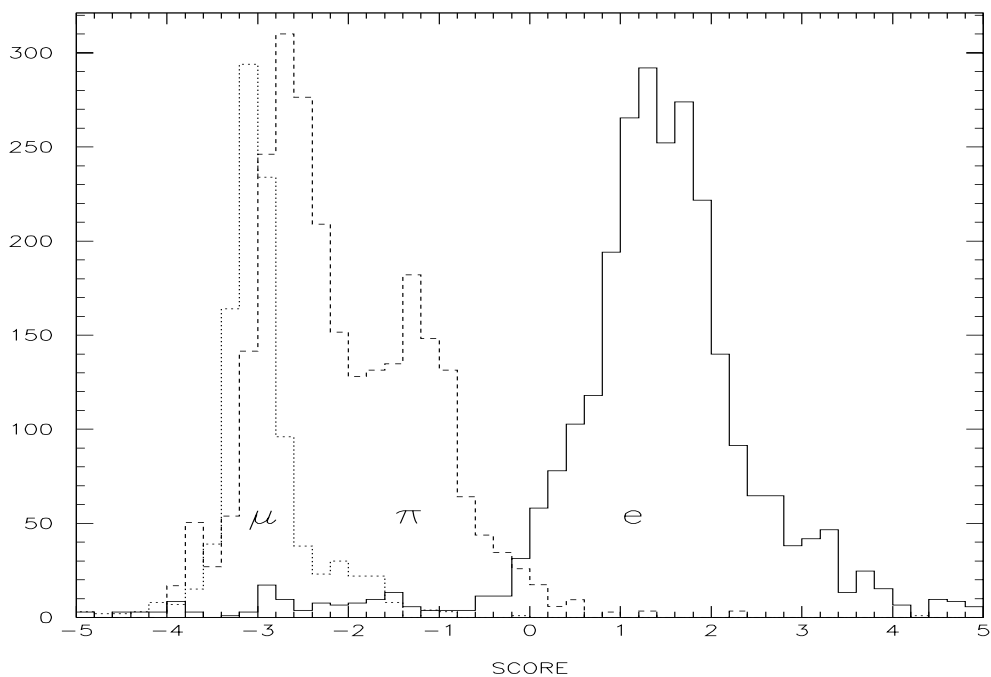
10

Figure 8: Some Discriminant Variables for e, π and μ.

11

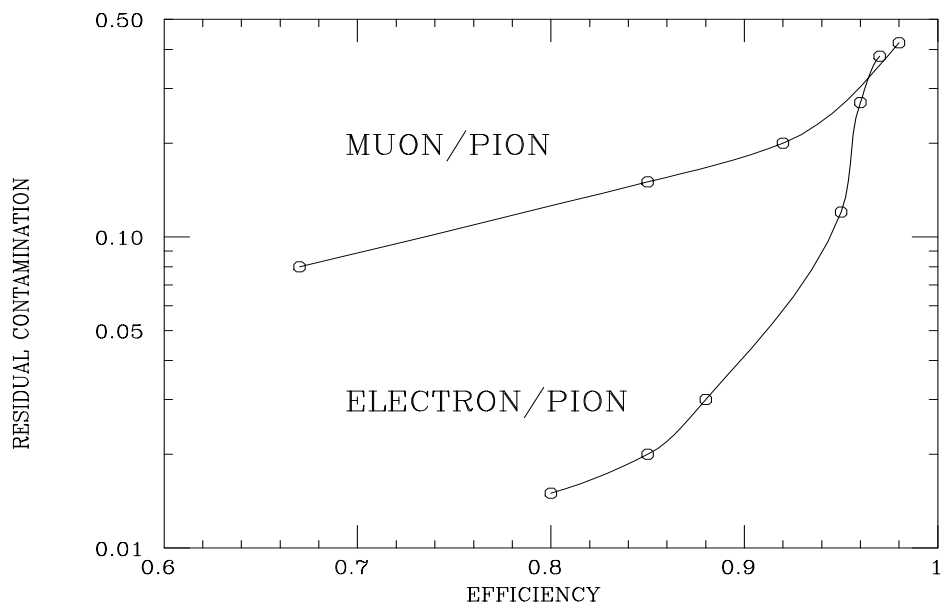Outer em electron/pion/muon ID in the OE

Figure 9: a) Distribution of the score variable S for electron, muon, and pion training samples; b) efficiency and residual contamination for electron/pion and muon/pion identification.
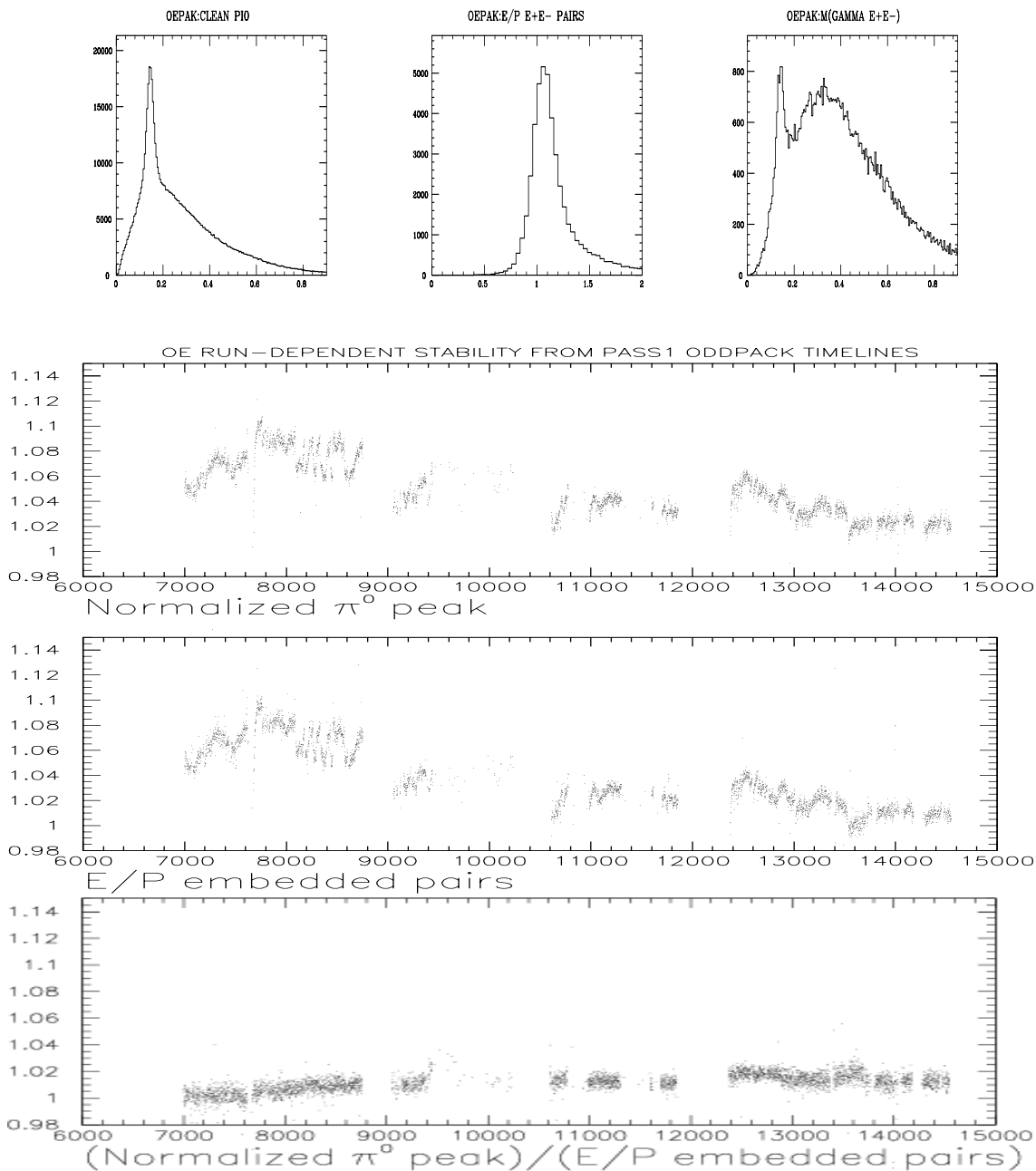
Figure 10: Long-term detector stability over 18 months. (top, left to right) $\gamma\gamma$ invariant mass distribution with the π^0 peak, E/P distribution, and $\gamma e^+ e^-$ invariant mass distribution with the π^0 peak. (bottom) Timelines, as a function of run number (typically one run per hour), of the E/P and π^0 peak, and the E/P peak corrected by the π^0 peak. After correction, the detector response is stable within $\pm 1\%$. The residual shift is compatible with the stability of the charged track spectrometer.

13

18-month data-taking period. Work is in progress to study process (3) (Fig.10 c), which will provide on an event-by-event basis the photon energy calibration constant, electron and positron E/P, and a check of the stability of the measurement of P, as performed by the magnetic spectrometer.

9   Physics results

Clean signals of the decays of charm mesons and baryons in many channels have been obtained by using the Outer em electron and muon identification and the π^0 reconstruction (Fig.11).

The geometrical acceptance of the Outer em for electrons and muons from semileptonic charm decays is about 30%, extending especially in the low-momentum region $P \sim 4\,\mathrm{GeV/c}$. The detection of charm semileptonic decays with the electron momentum in the acceptance of the Outer em is of particular interest in view of the possibility of determining the q^2 dependence for the formfactors (see, eg, Ref.[10] for an updated review). Studies performed in E687 include the Cabibbo-suppressed semileptonic decay $D^0 \rightarrow \pi^- e^+ \nu_e$ (Ref.[11]). The efficiency of μ/π rejection was measured on J/ψ decays where the muons were identified by the Outer muon counters, and found to be better than 80% from 5 to 50 GeV/c (Fig.11a). For the μ/π rejection, similarly to the case of e/π, the contribution of the Outer em is effective especially in the low momentum region (Fig.11b), as measured on pions from K_s decays.

Numerous charm decays have been found with π^0's reconstructed by the Outer em (Fig.11c-m). Thanks to the large statistics and low level of background, precision measurements such as the isospin mass splittings $m(D^{*+}) - m(D^{*0})$ of excited charm meson states have been initiated. Preliminary results[13] (Fig.11e) show how well the attainable precision compares with the best results obtained by e^+e^- experiments using crystal calorimetry[14].

In conclusion, the ten-year operational experience of the Outer em calorimeter of FOCUS shows how a detector based on conventional techniques is able to perform consistently and provide competitive physics results. The implementation of a scintillator tile tiebreaker has increased shower reconstruction efficiency in the small-angle region, and has considerably cleaned the π^0 peak of spurious combinations. Long-term response stability of 1% is attained by cross-calibration between E/P for electrons and π^0 peaks in hadronic events, while Discriminant Analysis is used to provide e/π and μ/π identification.
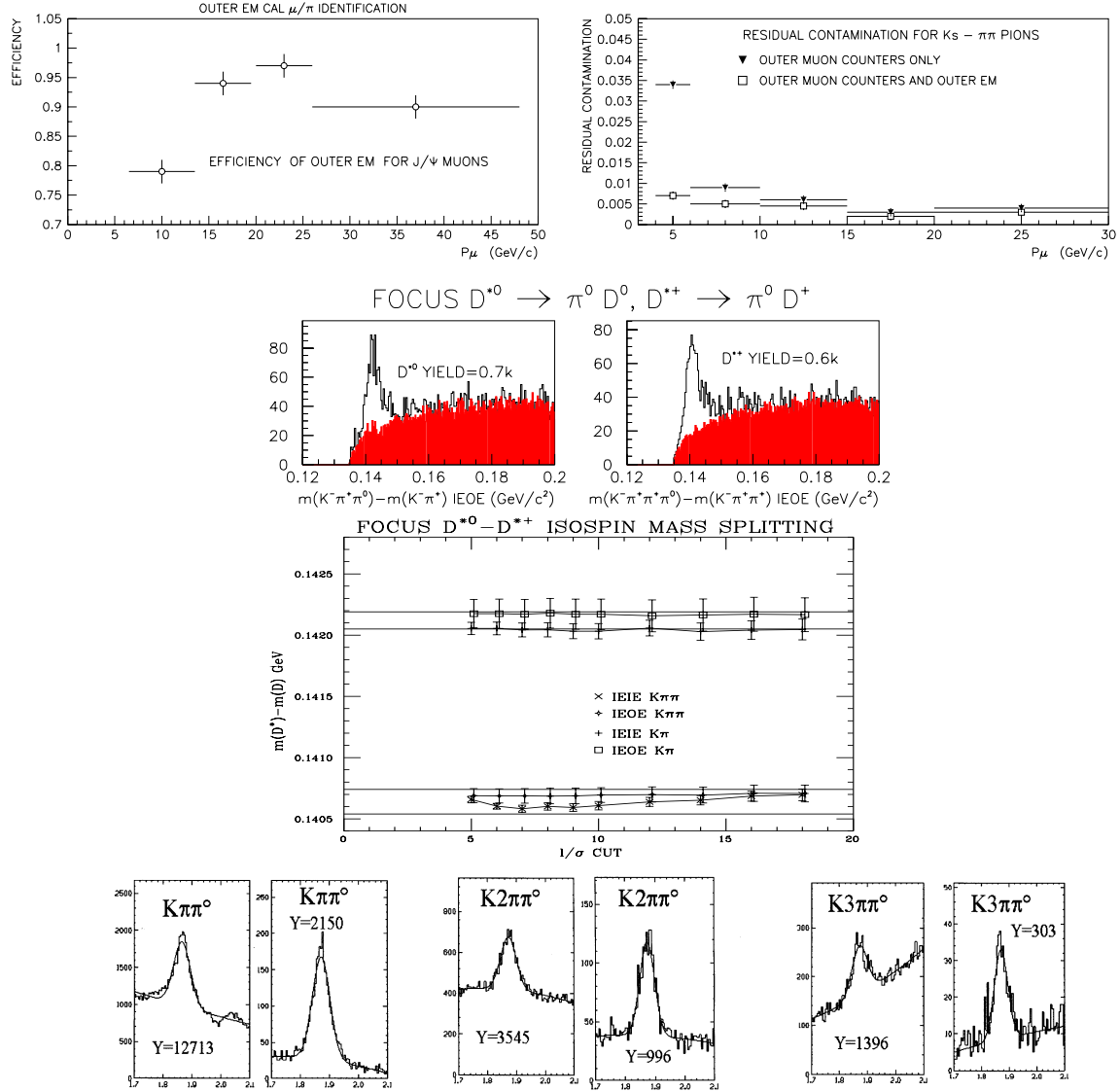
Figure 11: FOCUS preliminary results on a fraction of the 1996-97 dataset. From top to bottom: efficiency on muons from $J/\psi \rightarrow \mu^+\mu^-$ and rejection of pions from $K_s \rightarrow \pi^+\pi^-$; D^{*0} and D^{*+} decays with π^0 in the final state, and comparison of the precision attainable on the isospin mass splittings compared to world average, as functions of detached vertex significance ℓ/σ; several decays of D^+ and D^0 mesons with π^0 in the final state, with a selection of preliminary background-reducing cuts.

Acknowledgements

References

[1] P.L. Frabetti *et al.*, Nucl. Instrum. and Meth. **A320**, 519 (1992).

[2] S. Bianco *et al.*, Frascati preprint LNF-85-49-R.

[3] G. Bologna *et al.*, Nucl. Instr. and Meth. **192** (1982) 315.

[4] G. Apollinari, D. Scepanovic and S. White, Nucl. Instrum. and Meth. **A311**, 520 (1992).

[5] G.A. Akopdjanov *et al*, Nucl. Instr. and Meth. **140**, 441 (1977).

[6] Various Authors, Statistical Package for the Social Sciences (SPSS), McGraw-Hill, New York (1975).

[7] I. Nakano and K. Miyake, Jap. J. Appl. Phys. **24**, 506 (1985).

[8] G. Gianini, *The space variables in the π^0 energy estimate*, FOCUS internal report E831-mem-1998/7.

[9] S. Bianco *et al.*, Nucl. Instrum. and Meth. **A305**, 48 (1991).

[10] S. Bianco, invited review at the XIX Physics in Collision, Ann Arbor (USA), June 1999, hep-ex/9911034.

[11] P.L. Frabetti *et al.* Phys. Lett. **B382**, 312 (1996).

[12] P.L. Frabetti *et al.* Phys. Lett. **B331**, 217 (1994).

[13] J.Wiss [for the FOCUS Collaboration], APS Centennial meeting, May 1999, Atlanta (USA).

[14] D. Bortoletto et al. PRL 69 (1992) 2046.